Appl Phys A (2011) 102: 367–371
DOI 10.1007/s00339-010-6011-7

Applied Physics A
Materials Science & Processing

Room-temperature ferromagnetism of diamagnetically-doped ZnO aligned nanorods fabricated by vapor reaction

ShaoMin Zhou · LiSheng Liu · ShiYun Lou · YongQiang Wang · XiLiang Chen · HongLei Yuan · YaoMing Hao · RuiJian Yuan · Ning Li

Received: 3 May 2010 / Accepted: 10 August 2010 / Published online: 31 August 2010

Abstract Large-scale monocrystalline oxide-diluted magnetic semiconductor (ODMS) $Zn_{1-x}Bi_xO$ nanorods arrays (NAs) were prepared within a large doping concentration range from 5% to 20% by a simple chemical vapor deposition. X-ray diffraction and high-resolution transmission electron microscopy reveal the monotonous expansion of the lattice constants with increasing Bi content, due to the effective Bi doping. In particular, room-temperature ferromagnetic (RTFM) behavior with Curie temperature over 363.7 K has been observed based on Bi-doped ZnO nanoarrays, whereas undoped ZnO NAs disappear. The RTFM origin is suggested, in which vacancies can be controlled to tune the FM. The as-formed RTFM NAs would have potential applications in many areas of advanced nanotechnology, such as new spintronic devices and magneto-optic components.

1 Introduction

Future new spintronic devices are expected to have small sizes, high performance, and high operation speeds, and nanoarrays are believed to be the appropriate media to realize these goals [1, 2]. The modification of ZnO properties by impurity/dopant incorporation has become an important research topic recently, particularly for electronic, optical, and spintronic fields [3–13]. ZnO arrays of hierarchical assembly of nanoscale building blocks such as nanocomb/nanocantilever and nanorod arrays are a crucial step toward realization of functional nanosystems and represent a significant challenge in the field of nanoscale science [1–6]. The search for the RTFM in ODMSs has been intense in recent year [6–13]. However, the origin of RTFM, whether it arises from an intrinsic property or impurity phase, is still under debate [6–13]. In order to circumvent the problem of magnetic precipitates in an ODMS, diamagnetic element (DE) doping has become an attractive approach where ZnO: DE has the possibility of being free of FM precipitates and hence forms unambiguous evidence since the elements and their oxides are nonmagnetic [10–12]. Recently, it has been reported on RTFM of DE-doped ZnO nanowires, including C [10], Cu [11], and Bi-Cu [12]. However, synthesis and magnetic properties of Bi-doped ZnO NAs have been limited although preparation and corresponding optical properties have just been studied [13–15]. Previously, we have fabricated ferromagnetically doped ZnO nanocombs/cantilevers and tunable optical properties [4, 5, 16], as well as more recently tailored their magnetic properties [6, 17]. Bi has maximal RT diamagnetic constant in all elements and is also useful for low-temperature preparation of ZnO nanorods due to its low melting point (271.3°C at 1 atm) [13–15]. In the work, we firstly report a comparative examination of the ferromagnetism in undoped and Bi-doped as-grown ZnO NAs fabricated by a low-temperature chemical vapor transport reaction route since high temperature is not well suited to other processing techniques. In particular, RTFM of the as-synthesized products has been distinctly observed in Bi-doped ZnO NAs but not in undoped ones. These results demonstrate a step toward the use of one-dimensional ZnO NAs as building blocks for the bottom-up construction of RTFM ODMS nanodevices.

S. Zhou (✉) · L. Liu · S. Lou · Y. Wang · X. Chen · H. Yuan · Y. Hao · R. Yuan · N. Li
Key Lab for Special Functional Materials of Ministry of Education, Henan University, Kaifeng 475004, China
e-mail: smzhou@henu.edu.cn

2 Experimental

The synthetic routes of $Zn_{1-x}Bi_xO$ ZnO NAs samples are similar to our earlier reports [3–6, 17]. All the NAs in this part of our study were grown at 300°C, in an Ar ambient and a deposition pressure of ~90 Torr whereas only the Bi content of the NAs was varied. In a typical experiment, we used $Zn(NO_3)_2$ and $Bi(NO_3)_3$ powders (nominal ratios of Zn to Bi are 100:0, 95:5, 90:10, 85:15, and 80:20, respectively, and the total of them is 100.0 g) as starting materials without the presence of a premeditate catalyst. The whole growth process was carried out in a horizontal electronic resistance furnace, which was heated by silicon–carbon rods. According to the following ratios (the ratio of starting materials is the key factor to the quantity of Bi-doped in the NAs). Starting materials were put in the front of an alumina boat, which was covered with a quartz plate to maintain a local higher pressure reaction. The alumina boat was placed in the middle of the quartz tube that was inserted in the furnace. Prior to heating, the system was flushed with high-purity Ar for 5 hours to eliminate air. Then, under a constant flow of ammonia gas 80 sccm and vacuum conditions (~90 Torr), the furnace was rapidly heated to 300°C, and held at the temperature for 30 min. After the system was cooled down to RT, a large piece of wool-like products were seen in the alumina boat. The phase of as-synthesized products was studied by X-ray diffraction (XRD, Philips). The morphologies and sizes of the samples were characterized by using scanning electron microscopy (SEM) [XL 30-S-FEG, Philips, equipped with X-ray energy diffraction (EDX)]. A little of the products obtained so was ultrasonically dispersed in ethanol and a drop of this sample was deposited on a holey copper grid with carbon film, and then characterized by high-resolution transmission electron microscopy (HRTEM) (JEOL 2010, equipped with selected area electron diffraction (SAED), Japan). Magnetism measurements were carried out by using MPMS-XL5 at temperatures between 4 and 375 K. The contribution of the substrate to the magnetic measurements was subtracted by placing long strips of the substrate material, the same width as the sample, both above and below the sample such that a representative portion of the substrate material was always within the pick-up coils.

3 Results and discussion

The as-grown comb-like Bi (20%)-doped ZnO nanoarrays, mostly lying on the Si substrate surfaces, are depicted in a typical SEM image [Fig. 1(a)]. The inset figure is for a high-resolution (HR) SEM image (HRSEM) taken from a white rectangle area marked in Fig. 1(a). The lengths of nanocombs are up to several micrometers,

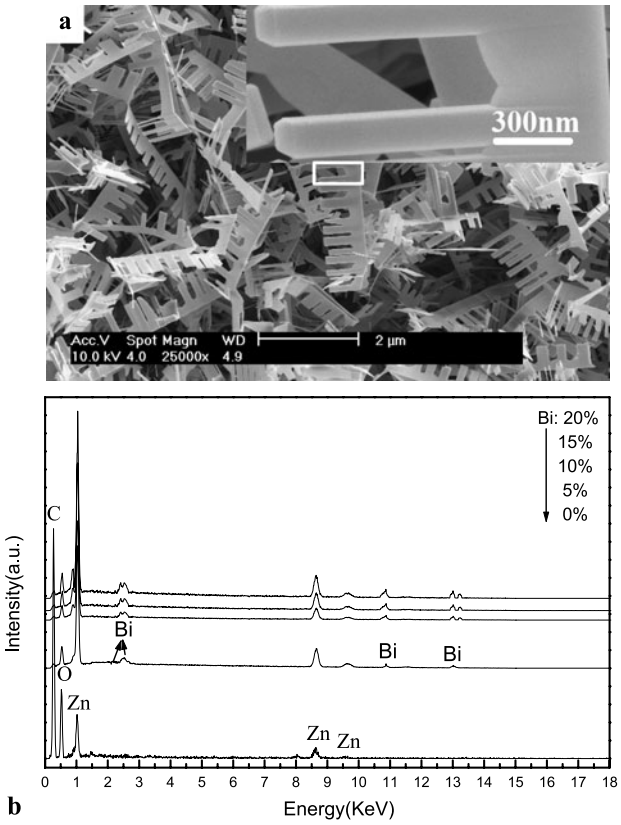

Fig. 1 (**a**) A SEM image of Bi(20%)-doped ZnO NAs and HRSEM image (*inset*); (**b**) EDX of five products

in which their branches are composed of rod-like nanostructures. Based on the HRSEM, each nanocomb/NA usually contains several tens of perfectly aligned and evenly spaced nanorods with almost constant diameter (60 nm) and spacing (150 nm), which are similar to our earlier reports [3–6, 17]. The typical EDX patterns, taken from a single NA, are shown in Fig. 1(b) where C peak comes carbon film for the characterization of SEM and HRSEM, and every NA has almost the same composition and contains a small amount of Bi except undoped sample (the bottom of Fig. 1(b)). Further quantitative analysis of five EDXs finds that the five kinds of atomic ratios between Zn and Bi are about 80:20($Zn_{0.8}Bi_{0.2}O$), 85:15($Zn_{0.85}Bi_{0.15}O$), 90:10($Zn_{0.9}Bi_{0.1}O$), 95:5($Zn_{0.95}Bi_{0.05}O$), and 100:0 (pure ZnO), respectively, which are compatible with nominal raw ingredients put in furnace. Figure 2(a) shows the XRD patterns of the $Zn_{0.8}Bi_{0.2}O$ NA samples, in which all diffraction peaks can be indexed to a hexagonal wurtzite structured ZnO. The XRD results also indicate a monotonic increase in the lattice constant with increasing Bi concentration, as can be seen in an inset of Fig. 2(a). Based on the most intense diffraction peak [0002], it is clear evidence with a slightly shift into low angular scale whereas corresponding intensity decreases compared with undoped ZnOs. The D-space [0002] values monotonically enlarged

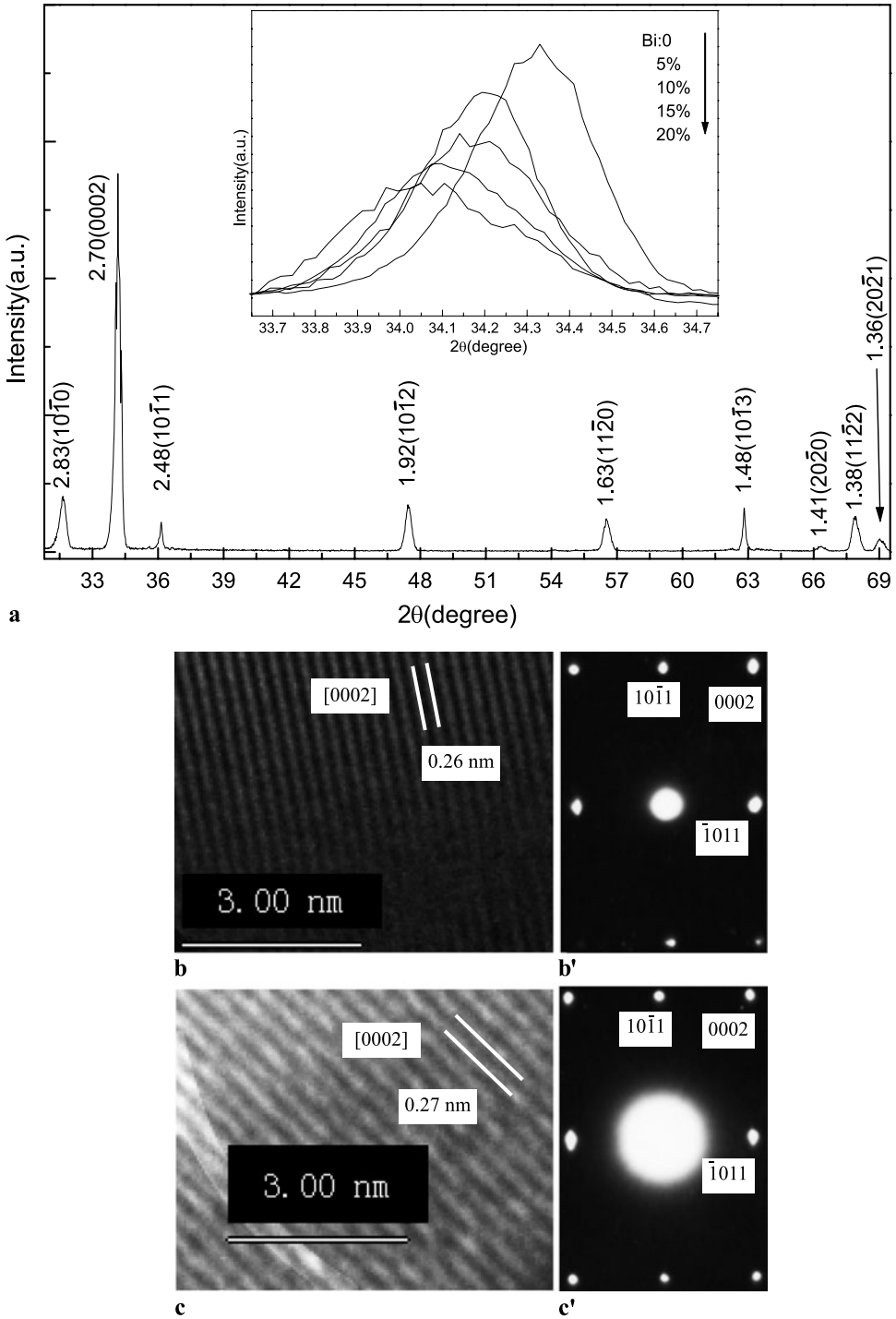

Fig. 2 (**a**) Full-range XRD patterns taken from the $Zn_{0.8}Bi_{0.2}O$ and high-resolution XRD of all samples (*inset*); (**b**) HRTEM image and (**b′**) SAED pattern of ZnO NAs; (**c**) HRTEM image and (**c′**) SAED pattern of $Zn_{0.8}Bi_{0.2}O$ NAs

as the Bi concentration increased, which indicates that the Bi ions systematically substituted for the Zn ions in the sample without changing the wurtzite structure, which is due to the bigger covalent radius of Bi (1.5 Å) than that of Zn (1.3 Å) and more structural defects. The lattice parameter *c* calculated from the (0002) peaks of the samples is 2.7 Å ($Zn_{0.8}Bi_{0.2}O$), 2.69 Å ($Zn_{0.85}Bi_{0.15}O$), 2.67 Å ($Zn_{0.9}Bi_{0.1}O$), 2.65 Å ($Zn_{0.95}Bi_{0.05}O$), and 2.60 Å (ZnO), respectively. Therefore, the Bi atoms were separated by 5.20 Å along the c-axis instead of a-axis (3.25 Å). As shown in Fig. 2(b, c), both of representative HRTEM images of ZnO (b) and $Zn_{0.8}Bi_{0.2}O$ nanorod (c) are demonstrated, which are monolithically single crystalline and the space distances of between (0002) planes corresponds to ~0.26 nm and 0.27 nm. SAED patterns [Fig. 2(c′) for $Zn_{0.8}Bi_{0.2}O$ and Fig. 2(b′) for ZnO] show the same set of

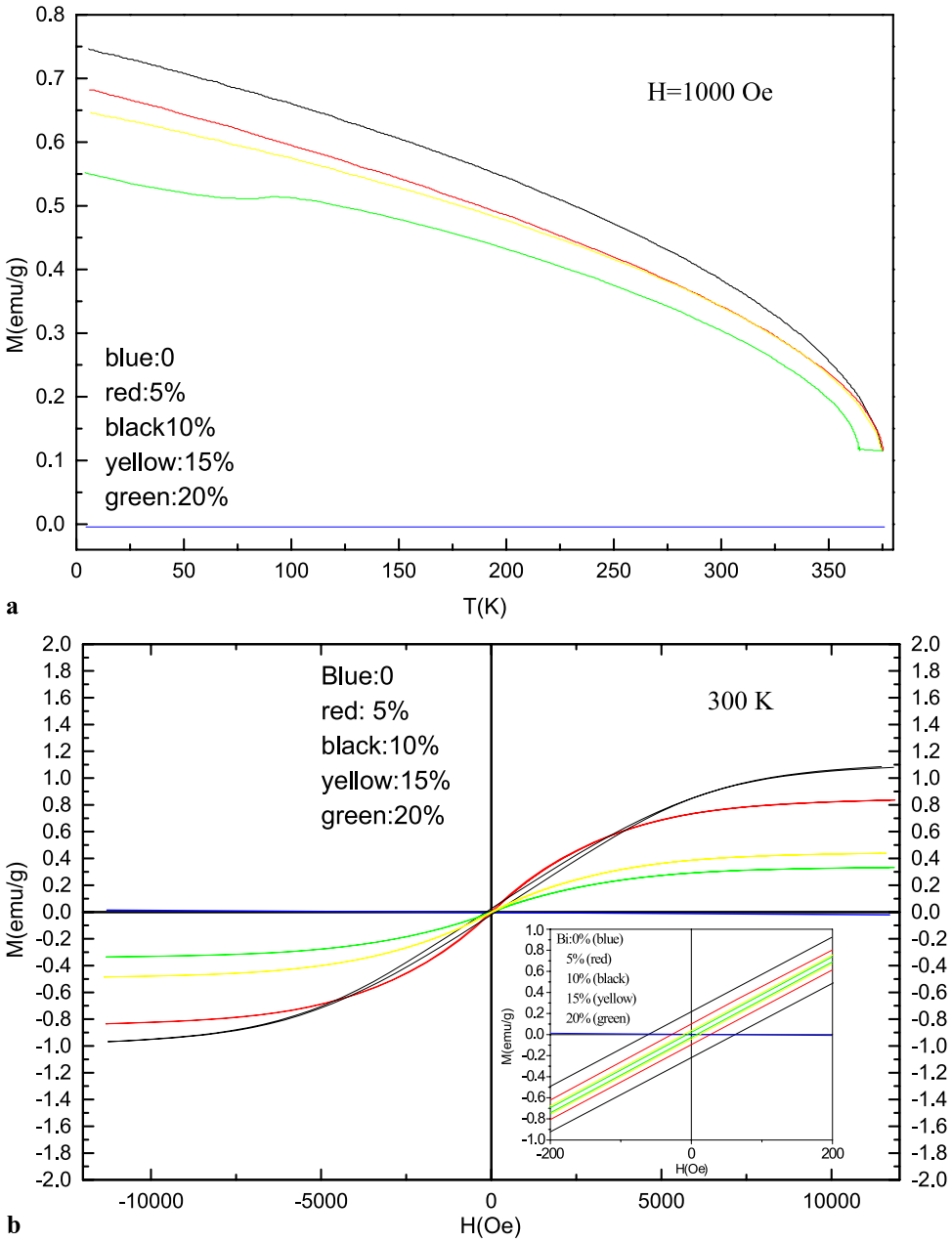

Fig. 3 (**a**) M–T curve [ZnO (blue, bottom), $Zn_{0.95}Bi_{0.05}O$ (red), $Zn_{0.9}Bi_{0.1}O$ (black), $Zn_{0.85}Bi_{0.15}O$ (yellow), $Zn_{0.8}Bi_{0.2}O$ (green)]; (**b**) magnetization hysteresis loops for five bulk NAs at 300 K

spots with the $[2\bar{1}\bar{1}0]$ zone axis of ZnO, which can both be indexed as wurtzite hexagonal structure and no secondary phase was observed. The results of HRTEM and SAED are agreement with the XRD results.

Figure 3(a) depicts magnetization as a function of temperature (from 4 to 375 K) in an applied field (0.1 T) for five samples fabricated so [ZnO (blue, bottom), $Zn_{0.95}Bi_{0.05}O$ (red), $Zn_{0.9}Bi_{0.1}O$ (black), $Zn_{0.85}Bi_{0.15}O$ (yellow), $Zn_{0.8}Bi_{0.2}O$ (green)]. Magnetic measurements carried out on the pure ZnO NAs showed the expected diamagnetism with a negative magnetic susceptibility. Surprisingly, one finds diamagnetically doped $Zn_{0.8}Bi_{0.2}O$ showed spontaneous magnetization with $T_c = 363.7$ K, although it is the weakest magnetization in all doping ones. For other four doping samples, the lack of ferromagnetic transition in the M–T curves may indicate their T_c in excess of the 375 K temperature limit of the SQUID apparatus used to make the measurements. Five typical M–H plots of as-synthesized NAs at 300 K were further shown in Fig. 3(b). For doping samples, evidence for ferromagnetism is observed in the M–H plots where only undoped one is short of hysteresis and coercivity (see inset Fig. 3(b)). At 300 K, remanence (M_r); saturation moment (M_s); and coercive field (H_c) of $Zn_{0.95}Bi_{0.05}O$, $Zn_{0.9}Bi_{0.1}O$, $Zn_{0.85}Bi_{0.15}O$, and $Zn_{0.8}Bi_{0.2}O$ are 0.103, 0.225, 0.041, 0.023 emu/g; 0.84, 1.08, 0.44, 0.24 emu/g; and 26.7, 61.8, 11.9, 7.0 Oe, respectively. These

RTFM are similar to those reported recently for our ferromagnetic element-doped ZnO NAs [6, 17] and Cu-doped ZnO nanowires [11–13]. In contrast, no obvious hysteresis loop and negative magnetization are observed in an undoped ZnO NAs sample, which is compatible with M–T data. Unlike earlier literature [5, 6, 10–12, 16–18], however, the observed ferromagnetism initially increased reaching a maximum in the 10–15% range and then gradually weakened, that is, at higher concentrations of Bi (>20%), magnetization drops off sharply.

Generally speaking, there are three possible origins of the ferromagnetism in $Zn_{1-x}Bi_xO$ that we should consider. The first is the carrier-induced ferromagnetism (RKKY or double exchange mechanism) that is often reported for the III–V semiconductors [6, 13]. The second one is the paramagnetism of bismuth oxides, including Bi_2O_4 and Bi_2O_3, well-known nonferromagnetic material. The third possible origin is the clusters. We discounted the second possibility because the magnitude of magnetization is too large to attribute to the weak ferromagnetism of paramagnetic oxides and because we cannot detect bismuth oxides phases in the XRD, HRTEM, and SAED. As for the third possibility, no clusters phase was observed in the XRD patterns and HRTEMs, and the lattice constant (c axis) systematically increased as Bi content increased. These observations indicate that the Bi ions systematically substituted for Zn sites without changing the wurtzite structure. Therefore, the presence of free carriers and localized spins is a prerequisite for the appearance of RTFM.

4 Conclusions

To summarize, undoped and diamagnetic elements-doped ZnO NAs have been fabricated by using a simple chemical vapor-deposition method, in which RTFM of doping samples has been observed and the maximum of M_s, M_r, and H_c is up to 1.08 emu/g, 0.225 emu/g, and 61.8 Oe, respectively. The low defect level in any of pure ZnO NAs is consistent with the observation of nonferromagnetism in undoped ZnO. We demonstrate a vapor process for controlled elemental doping during the nanocrystal growth, which may offer new opportunities in fundamental and applied research.

Acknowledgements This work was partially supported by the Program for Science & Technology Innovation Talents in Universities of Henan Province (No. 2008 HASTIT002), Innovation Scientists and Technicians Troop Construction Projects of Henan Province (No. 094100510015), and by the Natural Science Foundation of China under Grant No. 20971036.

References

1. M. Huang, S. Mao, H. Feick, H. Yan, Y. Wu, H. Kind, E. Weber, R. Russo, P. Yang, Science **292**, 1897 (2001)
2. Z. Wang, X. Kong, J. Zuo, Phys. Rev. Lett. **91**, 185502 (2003)
3. S. Zhou, X. Meng, X. Zhang, X. Fan, K. Zou, S. Wu, S. Lee, Micron **36**, 55 (2005)
4. B. Zhang, X. Zhang, H. Gong, Z. Wu, S. Zhou, Z. Du, Phys. Lett. A **372**, 2300 (2008)
5. B. Zhang, S. Zhou, H. Wang, Z. Du, Chin. Sci. Bull. **53**, 1639 (2008)
6. S. Zhou, P. Wang, S. Li, B. Zhang, H. Gong, Z. Du, Chin. Phys. Lett. **25**, 4446 (2008)
7. T. Fukumura, Z. Jin, A. Ohtomo, H. Koinuma, M. Kawasaki, Appl. Phys. Lett. **75**, 3366 (1999)
8. Y. Matsumoto, M. Murakami, T. Shono, T. Hasegawa, T. Fukumura, M. Kawasaki, P. Ahmet, T. Chikyow, S. Koshihara, H. Koinuma, Science **291**, 854 (2001)
9. D. Buchholz, R. Chang, J. Song, J. Ketterson, Appl. Phys. Lett. **87**, 082504 (2005)
10. H. Pan, J. Yi, L. Shen, R. Wu, J. Yang, J. Lin, Y. Feng, J. Ding, L. Van, J. Yin, Phys. Rev. Lett. **99**, 127201 (2007)
11. C. Xu, J. Chun, D. Kimb, B. Chon, T. Joo, Appl. Phys. Lett. **91**, 153104 (2007)
12. C. Xu, K. Yang, L. Huang, H. Wang, Appl. Phys. Lett. **130**, 124711 (2009)
13. C. Xu, K. Rho, J. Chun, D. Kim, Nanotechnology **17**, 011 (2006)
14. B. Aleman, P. Hidalgo, P. Fernández, J. Piqueras, J. Phys. D, Appl. Phys. **42**, 225101 (2009)
15. B. Karthikeyan, C. Sandeep, R. Philip, M. Baesso, J. Appl. Phys. **106**, 114304 (2009)
16. S. Zhou, X. Zhang, X. Meng, S. Wu, S. Lee, Appl. Phys. A **81**, 1647 (2005)
17. S. Zhou, H. Yuan, L. Liu, X. Chen, S. Lou, Y. Hao, R. Yuan, Nanoscale Res. Lett. **5**, 1284 (2010)
18. D. Buchholz, R. Chang, J. Song, J. Ketterson, Appl. Phys. Lett. **87**, 082504 (2005)